

# Annealing temperature effect on structural, morphological and optical parameters of mesoporous TiO<sub>2</sub> film photoanode for dye-sensitized solar cell application

M. KHALID HOSSAIN<sup>1,5</sup>, M. F. PERVEZ<sup>1</sup>, M. N. H. MIA<sup>1</sup>, S. TAYYABA<sup>2</sup>, M. JALAL UDDIN<sup>3</sup>,  
R. AHAMED<sup>4</sup>, RUHUL A. KHAN<sup>1</sup>, M. HOQ<sup>1</sup>, MUBARAK A. KHAN<sup>1,\*</sup>, FARID AHMED<sup>5</sup>

<sup>1</sup>Atomic Energy Research Establishment, Bangladesh Atomic Energy Commission,  
GPO Box. 3787, Dhaka 1349, Bangladesh

<sup>2</sup>Dept. of Computer Engineering, The University of Lahore, Lahore 54000, Pakistan

<sup>3</sup>Dept. of Applied Physics, Electronics and Communication Engineering, Islamic University, Kushtia 7003, Bangladesh

<sup>4</sup>Dept. of Material Science and Engineering, University of Rajshahi, Rajshahi-6205, Bangladesh

<sup>5</sup>Department of Physics, Jahangirnagar University, Savar, Dhaka 1342, Bangladesh

Use of Degussa P25 titanium-dioxide nanopowder in dye-sensitized solar cell (DSSC) photoanode improves efficiency of the DSSC cell. Annealing of titanium dioxide is required for fabrication of crystalline mesoporous thin film photoanode on transparent conducting glass using doctor blade method. Different annealing temperatures provide different structural, morphological, and optical properties of the photoanode, which may influence the efficiency of the cell. In this paper, energy-dispersive X-ray spectroscopy (EDS), scanning electron microscopy (SEM), X-ray powder diffraction (XRD), and UV-Vis-NIR spectroscopic analysis have been carried out to investigate annealing temperature effect on various structural parameters, mole-fraction, phase-content, and optical bandgap of the TiO<sub>2</sub> film photoanode. It was observed that depending on annealing temperature, the ratio of polymorphs of Degussa P25 changed substantially. For the change in annealing temperature from 350 °C to 600 °C, variations occurred in crystallite size from 11.9 nm to 24.9 nm, strain from 0.006 to 0.014, specific surface area from 62.77 m<sup>2</sup>·g<sup>-1</sup> to 125.74 m<sup>2</sup>·g<sup>-1</sup>, morphology index from 0.49 to 0.64, dislocation density from 5 × 10<sup>13</sup> line/m<sup>2</sup> to 8 × 10<sup>15</sup> line/m<sup>2</sup>, crystallite per unit surface area from 2 × 10<sup>13</sup> m<sup>-2</sup> to 2.5 × 10<sup>14</sup> m<sup>-2</sup>, and optical bandgap from 2.4 eV to 3.1 eV.

Keywords: *TiO<sub>2</sub> photoanode; mesoporous TiO<sub>2</sub>; doctor blade method; Degussa P25; optical bandgap; spectroscopic analysis*

## 1. Introduction

Dye-sensitized solar cell (DSSC) provides low-cost, simple fabrication procedure, and promising efficiency. Thus, researchers have shown an increased interest in developing this kind of photovoltaic cell in recent years [1, 2]. DSSC comprises of three main components: photoanode, redox couple electrolyte, and counter electrode. In DSSCs, photogenerated charge carriers from dye molecules are collected by photoanode and counter-electrode material which transfer these charge carriers (electrons) to the outer circuit [3–5]. Crystal structure, specific surface ratio, grain size, traps, defects,

surface morphology, photocatalytic activity, optical properties, bandgap, etc. of the photoanode and counter-electrode play a crucial role in overall cell efficiency [4, 6]. Therefore, finding a new material and optimizing structural and optical properties of photoelectrode material are an active research area of photovoltaics to improve cell efficiency.

Different kinds of nanostructures e.g. mesoporous, mesoscopic spherical structures, nanorods, and nanowires, etc. of various organic and inorganic materials have been considered to employ as photoanodes [7]. Titanium dioxide, an n-type semiconductor, is one of those materials that have been applied to heterojunction solar cell (e.g. DSSC and all solid perovskite solar cells, etc.) as an electron transport layer because of its high

\*E-mail: makhan.inst@gmail.com

efficiency, low cost, chemical inertness, thermal and photo-stability [5]. Among various nanostructures, mesoporous materials having high specific surface area and ordered arrangement of uniform large-size pores [8] have gained extensive researchers' interest. Titanium dioxide ( $\text{TiO}_2$ ) is a wide bandgap material (about 3.2 eV), usually found in the form of anatase, rutile, and brookite [9, 10]. Anatase is more photoactive, has a greater band gap, higher refractive index, and higher electron diffusion coefficient than that of rutile [6]. But rutile is the most thermally stable polymorph [10]. In addition, anatase does not absorb blue light whereas rutile does a little amount. Because of higher bandgap, anatase offers higher cell voltage [11]. It has been reported that short-circuit photocurrent of the rutile-based cell is about 30 % lower than that of the anatase-based cell [5]. However, synergistic effect has been observed in the mixture of anatase and rutile nanoparticles. Enhanced photocatalytic effect and reduced recombination of photogenerated electron-hole pairs have also been observed [12]. Different ratios of these two polymorphs govern the efficiency of interfacial electron collection and transfer, demonstrating synergistic effect [4, 9, 13, 14].

To employ  $\text{TiO}_2$  as photoanode, conventionally, a mesoporous  $\text{TiO}_2$  photoanode is grown on transparent conducting oxide (FTO or ITO) fabricated by high-temperature sintering of  $\text{TiO}_2$  nanoparticles in the presence of pore-forming agents [7, 15]. Morphological structure and lattice parameters depend on precursor, process of synthesis, initial crystallite size [10, 16], and heat treatment. Degussa P25, a commercially available titanium dioxide nanopowder with 10 nm diameter particle (anatase to rutile 3:1) and doctor blade method have already gained popularity to grow mesoporous titanium dioxide on ITO coated glass [8, 17–19]. In this method, heat treatment is necessary to form crystalline structure [4]. It facilitates eliminating organic substances that might be present in the precursor paste as well as forming an electron transport network in sintered granular structure that has good contact with TCO substrate [19]. However, heat treatment results in a change

of micrograin structure, crystallinity, surface morphology, grain size, pore size, specific surface area, microstrain, dislocation density of the crystal, the ratio of polymorphs (particularly anatase and rutile because of phase transformation), etc. [10, 12, 20–22]. In turn, these changes also have an influence on photocatalytic activity, reflectance, diffusion reflectance, refractive index, work function of the particle surface, electron mobility, charge carrier lifetime and diffusion length affecting the cell performance [19, 20].

In doctor blade method, some additional chemicals are required to form a paste along with  $\text{TiO}_2$  nanopowder. The amount and types of chemicals influence photoanode properties as well. In this study, we made  $\text{TiO}_2$  paste with unique chemical combination that was found in previous studies [23, 24] to form an efficient photoanode. However, there has been no report why this particular combination of chemicals along with specific annealing temperature provide higher efficiency cell. Therefore, thorough characterization of the  $\text{TiO}_2$  photoanode is required to understand the influence of annealing temperature and chemical constituents on its performance.

The objective of this research work is to characterize  $\text{TiO}_2$  photoanode mesoporous film for various annealing temperatures to understand the effect of change in structural and optical properties obtained in this procedure. EDS, XRD, SEM, and UV-Vis-NIR spectroscopic characterization were carried out. EDS was used to verify titanium and oxygen content and absence of other contaminations to maintain the quality of the samples. SEM images show surface morphology of the photoanode film and XRD reveals structural parameters crystallite size, strain, morphology index (MI), specific surface area (SSA), mole fraction and phase content, dislocation density, and crystallites per unit surface area for different annealing temperatures. UV-Vis-NIR spectroscopic analysis reveals the effect of annealing temperature on absorption, transmittance, and optical bandgap of the  $\text{TiO}_2$  photoanode film.

## 2. Experimental

### 2.1. Materials

The following materials were used to prepare the mesoporous TiO<sub>2</sub> films for photoanode: indium tin oxide (ITO) coated glass plate (Dyesol, Australia) as substrate materials, TiO<sub>2</sub> nanopowder (Degussa P25, USA), titanium IV isopropoxide (TTIP) (Merck, Germany), Triton X-100 (Merck, Germany), polyethylene glycol (PEG) and citric acid (C<sub>6</sub>H<sub>8</sub>O<sub>7</sub>).

### 2.2. TiO<sub>2</sub> film coating for DSSC photoanode

At first, in a beaker the following materials were mixed properly by hand with the help of a glass rod for few minutes: 0.1 g of TiO<sub>2</sub> nanopowder (Degussa P25), 0.2 mL titanium (IV) isopropoxide, 0.1 mL citric acid (0.1 M), 0.05 mL Triton X-100, and 0.1 mL PEG. Then, to formulate more uniform homogeneous TiO<sub>2</sub> paste, previous procedure was repeated [23, 24]. Then, the TiO<sub>2</sub> coated ITO glass substrates (1 cm<sup>2</sup>) were annealed at 300 °C, 350 °C, 400 °C, 450 °C, 500, and 600 °C for 1 hour [23, 24]. After heat treatment, the substrates were allowed to cool slowly. Eventually, mesoporous photoanode of 10 μm was obtained.

### 2.3. XRD characterization

Various structural parameters of the TiO<sub>2</sub> photoanode developed on ITO coated glass substrates at different annealing temperatures (Ta = 300 °C, 350 °C, 400 °C, 450 °C, 500 °C and 600 °C) were investigated by X-ray diffractometer (GBC-EMMA, Australia) at 2θ position (from 20° to 90°) with CuKα X-ray of wavelength λ = 1.54056 Å.

### 2.4. SEM and EDS characterization

EDS and SEM characterizations were carried out by FESEM (JEOL JSM-7600F, Japan) at 5 kV to 7 kV accelerating voltage.

### 2.5. UV-Vis-NIR analysis

UV-Vis-NIR spectra of TiO<sub>2</sub> films annealed at different temperatures were recorded by UV-Vis-NIR spectroscopy (Hitachi 4200, Japan)

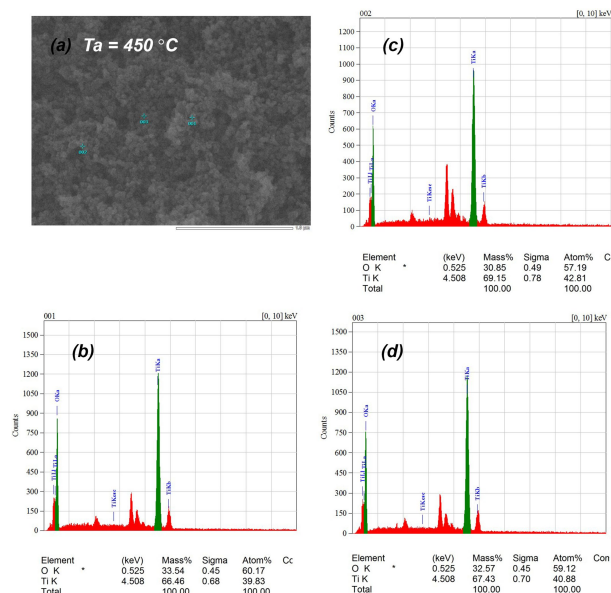


Fig. 1. EDS spectrum and distribution of elements for TiO<sub>2</sub> nanoparticles at 450 °C, for points denoted in Fig. 1(a) as 001 (b), 002 (c) and 003 (d).

in the range of 300 nm to 1100 nm, with a fresh ITO substrate used as a reference.

## 3. Results and discussion

### 3.1. EDS analysis

Energy dispersive spectroscopy (EDS) characterization is a method to determine percentage of various individual elements in a compound material by measuring the amplitude of wavelength of an X-ray emitted after hitting a sample by electron beam. In this research, EDS was used to assess the percentage of various elements existing in the TiO<sub>2</sub> films. The EDS images of TiO<sub>2</sub> films are shown in Fig. 1. EDS data were collected from three points of each sample specified in the SEM image which were identified as 001, 002 and 003 (Fig. 1). The atoms were recognized by determining the kinetic energy of emitted electrons from the atoms. The intense two peaks at 0.525 keV and 4.508 keV indicate the presence of oxygen atom (O) and titanium atom (Ti), respectively. Thus, it provides crucial information about the purity of the prepared samples. It is seen from Table 1 that the average atomic mass percentage of TiO<sub>2</sub> films obtained from EDS

Table 1. Comparison of atomic mass percentage for TiO<sub>2</sub> obtained from EDS with theoretical value.

Atomic mass [%]	EDS calculation [%]				Theoretical value [%]
	Point 1	Point 2	Point 3	Average	
Titanium (Ti)	66.46	69.15	67.43	67.68	59.93
Oxygen (O)	33.54	30.85	32.57	32.32	40.07

analysis are 67.68 % for Ti and 32.32 % for O. These values are in agreement with the standard values of 59.93 % for Ti and 40.07 % for O in TiO<sub>2</sub> compound.

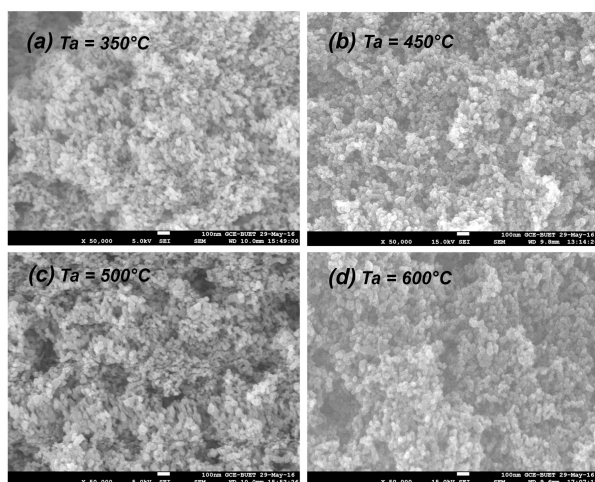


Fig. 2. SEM images taken after heat-treatment at (a) 350 °C, (b) 450 °C, (c) 500 °C and (d) 600 °C.

### 3.2. SEM analysis

SEM images (Fig. 2) of the prepared mesoporous TiO<sub>2</sub> film after heat treatment at four different temperatures (350 °C, 450 °C, 500 °C and 600 °C) were used to observe the surface morphology of TiO<sub>2</sub> film. Heat-treatment at different temperatures produced a subtle effect on surface morphology. It is seen that spherical nanoparticles of nanometer scale are agglomerated throughout the surface area. The particles that can be identified in nanometer scale are the primary particles, and agglomerations of several primary particles are termed as secondary particles. Various kinds of forces, e.g. capillary forces, weak surfaces forces (soft agglomerates), and strong

chemical bonds (hard agglomerates) cause agglomeration of small primary particles to form larger secondary particles.

### 3.3. XRD analysis

In Fig. 3, thirteen diffracted peaks for anatase phase A along with five peaks for rutile phase R are observed. The two intense diffracted peaks noticed for anatase and rutile are (1 0 1) and (1 1 0), respectively. These two phases dominate other phases substantially. Therefore, in this research, effect of annealing temperature on various structural parameters related to the performance of photoanode was analyzed for anatase (1 0 1) and rutile (1 1 0) phases.

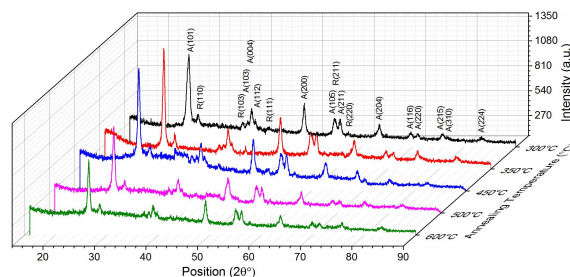


Fig. 3. XRD spectra of TiO<sub>2</sub> based photoanode at different annealing temperatures.

### 3.4. Effect of annealing temperature (Ta) on mole fraction and phase content

The existence of two phases (anatase and rutile) was established from the investigation of XRD peaks of the TiO<sub>2</sub> films. Molar ratio of anatase to rutile was calculated from the XRD peak intensity ratio by the method of Spurr and Myers [25] using the following formulas:

$$W_R = 1/[1 + 0.8(I_A/I_R)] \quad (1)$$

$$W_A = 1 - W_R \quad (2)$$

where  $W_A$  and  $W_R$  are the mole fractions of anatase and rutile, respectively;  $I_A$  and  $I_R$  are the peak intensities of anatase and rutile phases, respectively. Fig. 4 shows the impact of annealing temperature on mole fraction and phase content. It is seen that the change of the anatase phase and rutile phase is reciprocal to each other. At 350 °C annealing temperature, the content of the anatase phase is the highest whereas the content of rutile phase is the lowest. A subtle effect is observed for changing annealing temperature between 450 °C and 500 °C. In this region, the ratio of anatase to rutile is about 3:1. This ratio of anatase to rutile is similar to the ratio of anatase to rutile present in TiO<sub>2</sub> Degussa P25 nanopowder. Therefore, annealing temperature provides an effective mechanism to control molar fraction and phase content of anatase (1 0 1) and rutile (1 1 0) polymorph.

### 3.5. Effect of annealing temperature (Ta) on crystallite size and strain

Lattice strain is a measure of distribution of lattice constants originated from crystal distortion. Crystal imperfections such as lattice dislocation, grain boundary triple junction, contact or sintering stresses, coherency stresses, stacking faults, etc. are the sources of strain. Imperfection in crystal causes broadening of X-ray diffracted peaks [26]. Broadening of X-ray diffracted peaks enables an estimation of crystallite size and lattice strain. Crystallite size  $L$ , the average size of the crystalline domains, was estimated by the following Debye-Scherrer equation [27]:

$$L = \frac{K\lambda}{\beta \cos\theta} \quad (3)$$

Lattice strain  $e$  was estimated by Williamson-Hall method [28] from the following equation:

$$e = \frac{\beta}{4 \tan\theta} \quad (4)$$

where  $\beta$  is the full width at half-maximum (FWHM),  $K$  is a constant taken as 0.9,  $\lambda$  is the wavelength of X-ray,  $\theta$  is the Bragg angle in degree. Table 2 shows the crystallite size of different anatase and rutile phases obtained for Degussa

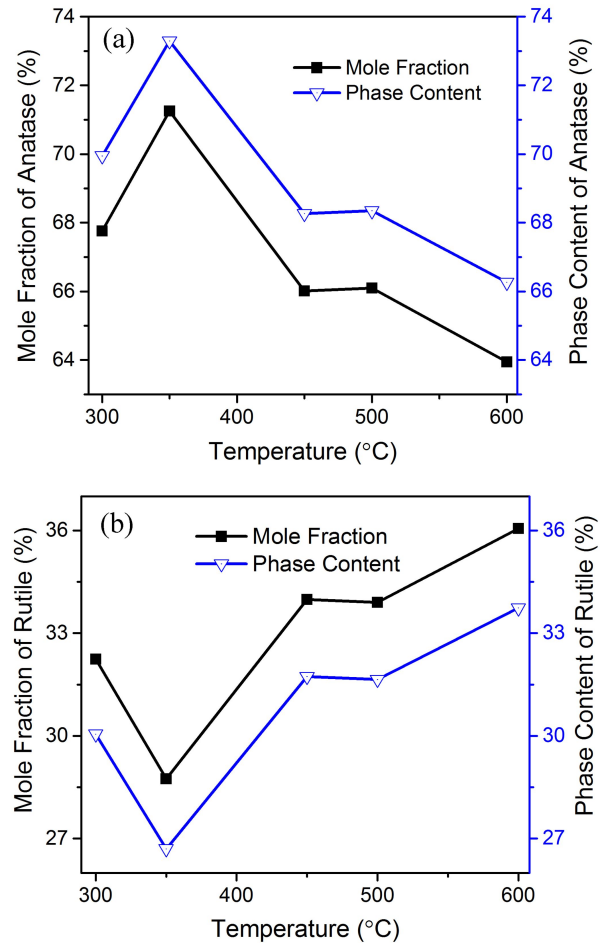


Fig. 4. Annealing temperature effect on mole fraction and phase content of (a) anatase (1 0 1) and (b) rutile (1 1 0) of Degussa P25 TiO<sub>2</sub>.

P25 TiO<sub>2</sub> film after annealing at different temperatures. It is observed that in XRD graph, there are no detectable peaks of R (2 1 1) phase at 500 °C, and R (2 2 0) phase at 500 °C and 600 °C. It is assumed that these phases are absent or not detectable by XRD and therefore, the crystallite size of these phases is not included in the table.

Fig. 5 shows a profound effect of annealing temperature on the crystal size and strain of anatase (1 0 1) and rutile (1 1 0) for Degussa P25 TiO<sub>2</sub>. For anatase phase (1 0 1), lattice strain rapidly decreased as the temperature increased from 300 °C to 350 °C. From 350 °C to 450 °C a subtle increase of strain is observed. Above 450 °C, strain decreased slowly till 600 °C. Crystallite size shows

Table 2. Crystallite size of various anatase (A) and rutile (R) phases at different annealing temperatures Ta.

Phase (A & R)	Crystallite size, L [nm]				
	Ta = 300 °C	Ta = 350 °C	Ta = 450 °C	Ta = 500 °C	Ta = 600 °C
A (1 0 1)	11.9	17.4	17.1	17.5	18.8
R (1 1 0)	15.8	24.9	20.3	24.3	22.6
R (1 0 1)	13.6	19.6	13.5	16.9	117
A (1 0 3)	13.4	27.7	17.7	36.29	20.0
A (0 0 4)	18.5	19.5	18	16.29	20.3
A (1 1 2)	32.3	45.2	26.8	25.1	21
R (1 1 1)	50.0	46.0	33.8	22.3	53.3
A (2 0 0)	17.6	16.7	16.6	10.6	19.5
A (1 0 5)	24.5	24.2	12.8	13.1	12.3
R (2 1 1)	42.3	110	124	–	–
A (2 1 1)	18.1	19.6	22.5	17.2	21.2
R (2 2 0)	24.0	64.2	17.0	19.12	
A (2 0 4)	14.8	16.6	11.2	23.2	16.7

exactly opposite trend. However, in the case of rutile phase (1 1 0), an irregular change of lattice strain and crystallite size is observed.

### 3.6. Effect of annealing temperature on specific surface area (SSA)

Characteristics of surface area are influenced by the large surface to volume ratio of nanoparticles. Inverse correlation between crystallite size and specific surface area (SSA) is observed. SSA can be calculated by taking into account the total area covered by the particles in a unit mass [29]. With the help of the equation 5, we can measure the SSA:

$$SSA = \frac{6 \times 10^3}{\rho D_p} \quad (5)$$

where  $\rho$  = nanoparticles density (here for TiO<sub>2</sub> its value is 4.23 g·cm<sup>-3</sup>),  $D_p$  = nanoparticles size. Fig. 6 shows the effect of annealing temperature on SSA. SSA for anatase phase changes from 75.60 m<sup>2</sup>·g<sup>-1</sup> to 125.74 m<sup>2</sup>·g<sup>-1</sup> and for rutile phase from 62.77 m<sup>2</sup>·g<sup>-1</sup> to 89.75 m<sup>2</sup>·g<sup>-1</sup>. It is seen that for both anatase and rutile phase SSA is decreasing till 350 °C. Above this temperature, an irregular change of SSA occurs. Around 450 °C, SSA reaches a peak value. Physical and chemical activity of nanoparticles depend on SSA playing a critical role in dye adsorption, heterogeneous catalysis

and reactions on the surface. As crystallite size decreases, SSA and surface to volume ratio increases dramatically [30, 31]. Higher surface area adsorbs more dye, increasing surface reactivity which, in turn, increases the efficiency. Therefore, SSA graph with annealing temperature provides crucial information for TiO<sub>2</sub> photoanode preparation.

### 3.7. Effect of annealing temperature on morphology index (MI)

With the help of equation 6, MI can be measured from full width at half maximum (FWHM) of X-ray diffraction (XRD) peaks [32]:

$$MI = \frac{FWHM_h}{FWHM_h + FWHM_p} \quad (6)$$

where  $FWHM_h$  = highest full width at half maximum FWHM value obtained from peaks,  $FWHM_p$  = particular peak full width at half maximum FWHM for which morphology index (MI) is to be measured.

Fig. 7 presents the effect annealing temperature on the morphology index for anatase (1 0 1) and rutile (1 1 0) phases. MI value swings with annealing temperature reaching the highest value between 450 °C to 500 °C annealing temperature.

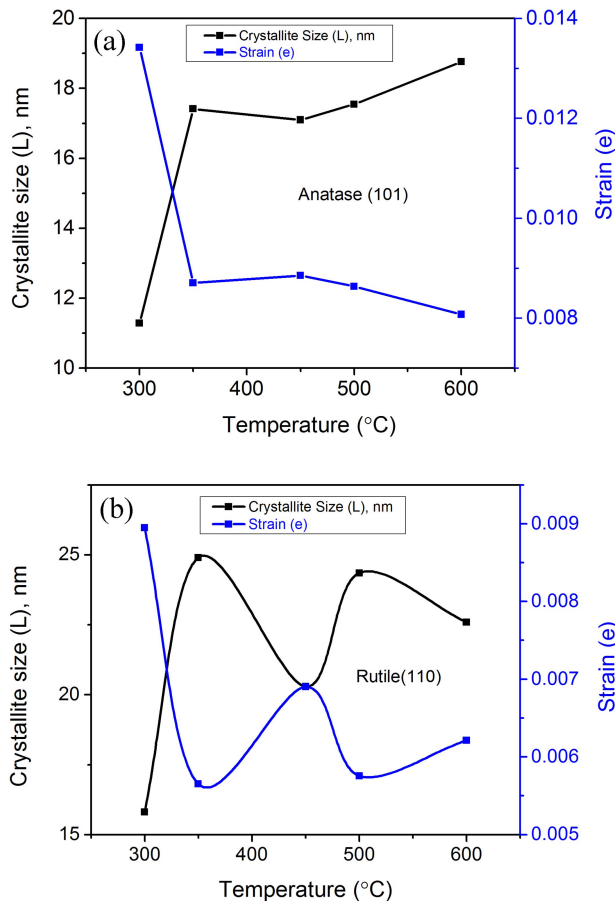


Fig. 5. Annealing temperature effect on crystal size and strain of (a) anatase (1 0 1) and (b) rutile (1 1 0), for Degussa P25 TiO<sub>2</sub>.

### 3.8. Effect of annealing temperature (Ta) on dislocation density and crystallites per unit surface area

During formation of crystals, dislocations originate from crystallographic defects (line defects) and irregularities. Mathematically, it is a type of topological defects. The term dislocation density is defined as the length of dislocation lines per unit volume of the crystal, and can be calculated by the following formula [33, 34]:

$$\delta = \frac{1}{L^2} \quad (7)$$

where L is the crystallite size.

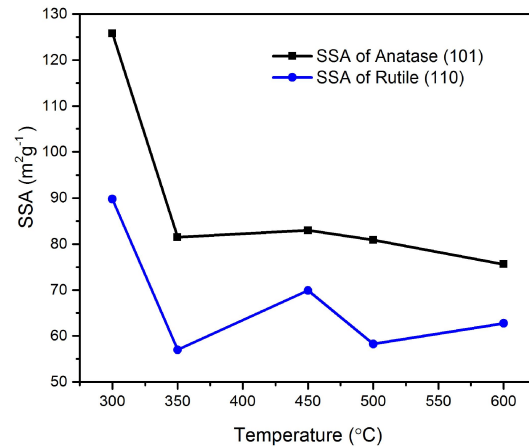


Fig. 6. Effect of annealing temperature on specific surface area (SSA).

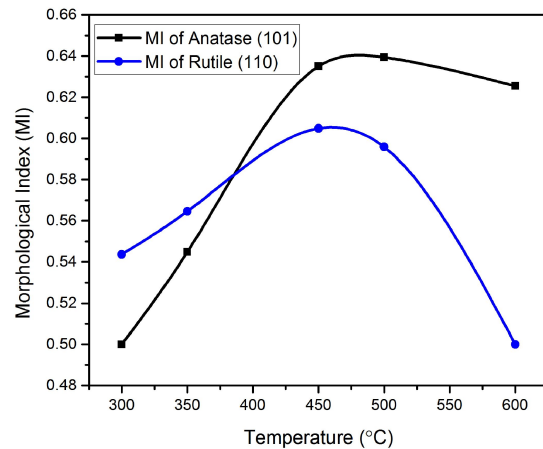


Fig. 7. Effect annealing temperature on morphology index.

Crystallites per unit surface area  $N$ , another important structural parameter, is determined by the following equation [34]:

$$N = \frac{d}{L^3} \quad (8)$$

where L is the crystallite size.

The variation of dislocation density and crystallites per unit surface area with annealing temperature of anatase (1 0 1) and rutile (1 1 0) for Degussa P25 TiO<sub>2</sub> are shown in Fig. 8. For anatase phase, it is seen that both dislocation density and crystallites per unit surface area decreased as the annealing temperature increased from 300 °C to 350 °C. For

the temperature in the range of 350 °C to 500 °C, the graph shows almost flat profile. For low temperature, the changes occur very rapidly, however, at high temperature, (above 450 °C) there is a gradual decrease in dislocation density and crystallites per unit surface area (Fig. 8a). Nevertheless, for rutile phase the changes in dislocation density and crystallites per unit surface area with the temperature occur irregularly. No constant change is observed for that case (Fig. 8b).

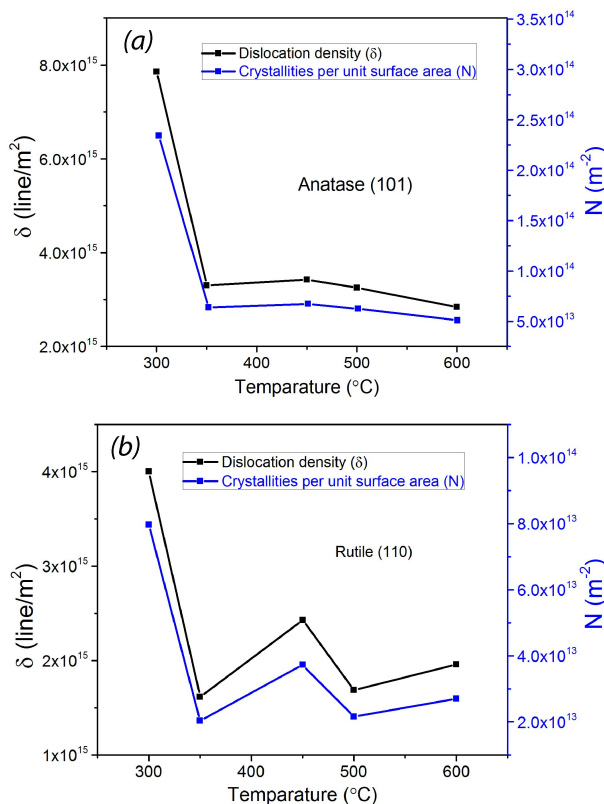


Fig. 8. Annealing temperature effect on dislocation density and crystallites per unit surface area of (a) anatase (1 0 1) and (b) rutile (1 1 0) for Degussa P25  $\text{TiO}_2$ .

### 3.9. Effect of annealing temperature on optical properties

Fig. 9 shows the effect of annealing temperature on transmittance, absorption, and optical bandgap. The measurements were carried out from 350 nm to 1100 nm wavelength range.

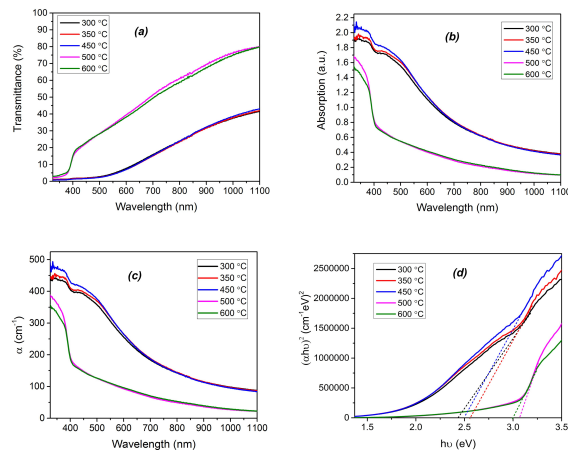


Fig. 9. (a) Transmittance spectrum (b) absorption spectrum (c) absorption coefficient and (d) optical bandgap of  $\text{TiO}_2$  film on ITO substrate.

Absorption coefficient is a parameter which is related to the light absorbing property of a material. It varies with wavelength of light and characteristics of the respective material. The absorption coefficient  $\alpha$  can be measured by using equation 9 [35] as:

$$\alpha = 2.303A/t \quad (9)$$

where  $A$  = absorbance,  $t$  = film thickness.

The optical bandgap can be determined by the Tauc formula [36] as:

$$(\alpha h\nu)^{1/n} = A(h\nu - E_g) \quad (10)$$

where  $\alpha$  = absorption coefficient,  $h$  = Planck constant,  $\nu$  = frequency of radiation,  $A$  = A constant,  $E_g$  = energy band gap.

From equation 10, direct bandgaps 2.45 eV, 2.55 eV, 2.5 eV, 3.05 eV and 3.0 eV were estimated for different annealing temperatures 300 °C, 350 °C, 450 °C, 500 °C and 600 °C, respectively, as shown in Fig. 9d. Higher annealing temperature produces larger size crystallite particles with lower specific surface area which in turn reduces scattering of light [37]. Thus, higher annealing temperature increases the transmittance, supporting the data of increasing the crystallite size found from XRD. Moreover, crystallite size plays a critical role in bandgap value along with the effect of mixture of different  $\text{TiO}_2$  polymorphs.

## 4. Conclusions

Effect of annealing temperature on structural, morphological and optical parameters of Degussa P25 titanium-dioxide DSSC photoanode has been investigated using XRD, EDS, SEM, and UV-Vis-NIR spectroscopic analyses. Phase content ratio of anatase (1 0 1) to rutile (1 1 0) in the material before annealing and after annealing is similar in the annealing temperature range of 450 °C to 500 °C. Above 350 °C, structural parameters: crystallite size, strain, specific surface area, dislocation density, and crystallite per unit surface area for anatase (1 0 1) deviate slowly, whereas mole fraction, phase content, and morphology index show dramatic change in the range of 350 °C to 450 °C. On the other hand, parameters variation of rutile phase (1 1 0) with annealing temperature occurs irregularly. However, between 450 °C to 500 °C, a subtle change occurs for both anatase (1 0 1) and rutile (1 1 0) phases. In this range, higher crystallite size, specific surface area, morphology index; and lower strain, dislocation density facilitate efficient charge collection and transfer, leading to more efficient solar cell performance. Moreover, substantial variation in optical properties transmittance, absorbance, and bandgap is noticed with changing annealing temperature.

## Acknowledgements

XRD and UV-Vis-NIR characterization were performed at IFRD, BSCIR, Bangladesh. SEM and EDS characterization were carried out at GCE, BUET, Bangladesh. The financial grant was provided by IDCOL and supported by MOST, Bangladesh. This entire work was carried out at IRPT, AERE, Bangladesh Atomic Energy Commission.

## References

- [1] O'REGAN B., GRÄTZEL M., *Nature*, 353 (1991), 737.
- [2] SALAM Z., VIJAYAKUMAR E., SUBRAMANIA A., SIVASANKAR N., MALLICK S., *Sol. Energ. Mat. Sol. C.*, 143 (2015), 250.
- [3] GHANN W., KANG H., SHEIKH T., YADAV S., CHAVEZ-GIL T., NESBITT F., *Sci. Rep.-UK*, 7 (2017), 41470.
- [4] JUNG Y.H., PARK K.-H., OH J.S., KIM D.-H., HONG C.K., *Nanoscale Res. Lett.*, 8 (2013), 37.
- [5] BAI Y., MORA-SERO I., ANGELIS F.D., BISQUERT J., WANG P., *Chem. Rev.*, 114 (2014), 10095.
- [6] ROGERS K.D., LANE D.W., PAINTER J.D., CHAPMAN A., *Thin Solid Films*, 466 (2004), 97.
- [7] GARMAROUDI Z.A., MOHAMMADI M.R., *J. Sol-Gel Sci. Techn.*, 76 (2015), 666.
- [8] ANDRONIC L., PERNIU D., DUTA A., *J. Sol-Gel Sci. Techn.*, 66 (2013), 472.
- [9] LIU L., CHEN X., *Chem. Rev.*, 114 (2014), 9890.
- [10] LI W., NI C., LIN H., HUANG C.P., SHAH S.I., *J. Appl. Phys.*, 96 (2004), 6663.
- [11] HART J.N., MENZIES D., CHENG Y.-B., SIMON G.P., SPICCIA L., *Sol. Energ. Mat. Sol. C.*, 91 (2007), 6.
- [12] BESSERGENEV V.G., MATEUS M.C., REGO A.M.B.D., HANTUSCH M., BURKEL E., *Appl. Catal. A-Gen.*, 500 (2015), 40.
- [13] WANG W.-K., CHEN J.-J., ZHANG X., HUANG Y.-X., LI W.-W., YU H.-Q., *Sci. Rep.-UK*, 6 (2016), 20491.
- [14] LI G., RICHTER C.P., MILOT R.L., CAI L., SCHMUTTENMAER C.A., CRABTREE R.H., BRUDVIG G.W., BATISTA V.S., *Dalton T.*, 0 (2009), 10078.
- [15] CHEN D., HUANG F., CHENG Y.-B., CARUSO R.A., *Adv. Mater.*, 21 (2009), 2206.
- [16] MATHEWS N.R., MORALES E.R., CORTES-JACOME M.A., ANTONIO J.A.T., *Sol. Energy*, 83 (2009), 1499.
- [17] OHNO T., SARUKAWA K., TOKIEDA K., MATSUMURA M., *J. Catal.*, 203 (2001), 82.
- [18] OHTANI B., PRIETO-MAHANEY O.O., LI D., ABE R., *J. Photoch. Photobio. A.*, 216 (2010), 179.
- [19] CHEN Y., STATHATOS E., DIONYSIOU D.D., *J. Photoch. Photobio. A.*, 203 (2009), 192.
- [20] RAJ K.J.A., VISWANATHAN B., *Indian J. Chem. A.*, 48A (2009), 1378.
- [21] RAJAMANICKAM A.T., THIRUNAVUKKARASU P., DHANAKODI K., *J. Mater. Sci.-Mater. El.*, 26 (2015), 8933.
- [22] TRIPATHI A.K., SINGH M.K., MATHPAL M.C., MISHRA S.K., AGARWAL A., *J. Alloy. Compd.*, 549 (2013), 114.
- [23] HOSSAIN M.K., PERVEZ M.F., TAYYABA S., UDDIN M.J., MORTUZA A.A., MIA M.N.H., MANIR M.S., KARIM M.R., KHAN M.A., *Mater. Sci.-Poland*, 2017 (Tentatively Accepted).
- [24] HOSSAIN M.K., PERVEZ M.F., MIA M.N.H., MORTUZA A.A., RAHAMAN M.S., KARIM M.R., ISLAM J.M.M., AHMED F., KHAN M.A., *Results Phys.*, 7 (2017), 1516.
- [25] SPURR R.A., MYERS H., *Anal. Chem.*, 29 (1957), 760.
- [26] ZAK A.K., MAJID W.H.A., ABRISHAMI M.E., YOUSEFI R., *Solid State Sci.*, 13 (2011), 251.
- [27] CULLITY B.D., STOCK S.R., *Powder Photographs*, in: COHEN M. (Ed.), *Elements of X-ray Diffraction*, Addison-Wesley, USA, 1956, p. 149.
- [28] BINDU P., THOMAS S., *J. Theor. Appl. Phys.*, 8 (2014), 123.
- [29] AKBARI B., TAVANDASHTI M.P., ZANDRAHIMI M., *Iran. J. Mater. Sci. Eng.*, 8 (2011), 48.
- [30] CHEN J., LI Y., WANG Y., YUN J., CAO D., *Mater. Res. Bull.*, 39 (2004), 185.
- [31] ZHANG J., XIAO X., NAN J., *J. Hazard. Mater.*, 176 (2010), 617.

- 
- [32] THEIVASANTHI T., ALAGAR M., *Chem. Phys.*, (2013), 1307.
- [33] KELLY A., KNOWLES K.M., *Crystallography and Crystal Defects*, John Wiley & Sons Ltd., Chichester, UK, 2012.
- [34] SALEEM M., *Int. J. Phys. Sci.*, 7 (2012), 2971.
- [35] MAJOR C., NEMETH A., RADNOCZI G., CZIGANY Z., FRIED M., LABADI Z., BARSONY I., *Appl. Surf. Sci.*, 255 (2009), 8907.
- [36] EL-NAHASS M.M., ALI M.H., EL-DENGLAWAY A., *T. Nonferr. Metal. Soc.*, 22 (2012), 3003.
- [37] KOLAY A., KUMAR P.N., KUMAR S.K., DEEPA M., *Phys. Chem. Chem. Phys.*, 19 (2017), 4607.

Received 2017-07-09

Accepted 2017-09-22